Journal of Solid State Chemistry **157,** 56–61 (2001)
doi:10.1006/jssc.2000.9038, available online at http://www.idealibrary.com on IDEAL®

HREM Study of Fluorinated Nd_2CuO_4

J. Hadermann[1] and G. Van Tendeloo

EMAT, University of Antwerp (RUCA), Groenenborgerlaan 171, B-2020 Antwerp, Belgium

and

A. M. Abakumov, M. G. Rozova, and E. V. Antipov

Department of Chemistry, Moscow State University, 119899 Moscow, Russia

Received July 31, 2000; in revised form October 24, 2000; accepted December 1, 2000

Nd_2CuO_4 was fluorinated using XeF_2 as a soft fluorinating agent at temperatures ranging from 200°C to 500°C. The structure of the fluorinated samples was studied using a combination of X-ray powder diffraction, electron diffraction, and high-resolution electron microscopy. Samples annealed in the temperature range of 300°C to 400°C reveal the formation of a new monoclinic phase ($a \approx 12.96$ Å, $b \approx 5.5$ Å, $c \approx 5.8$ Å, and $\beta \approx 92°$; space group $C2/c$). The structural model was deduced from electron microscopy investigations. It involves an ordered occupation of anion sites between two adjacent Nd layers by anions and anion vacancies and the partial migration of anions from these tetrahedrally coordinated fluorite-type positions to octahedral interstices forming apical vertexes of $Cu(O, F)_6$ octahedra. No superconductivity was observed for this new monoclinic phase. The relationships between the structures of fluorinated T, T′, and T* phases are discussed.

Key Words: **variable fluorination; Nd_2CuO_4; $Nd_2CuO_3F_5$; TEM.**

1. INTRODUCTION

The R_2CuO_4 cuprates of rare-earth elements are commonly regarded as an intergrowth of (CuO_2) sheets which represent the perovskite-like fragment and R_2O_2 blocks adopting either a rock-salt-type structure (T phase, R = La) or a fluorite-type structure (T′ phase, R = Pr–Gd). The R^{3+} cations in both cases form a close-packed arrangement. Only the octahedral interstices are filled by oxygen atoms in the T phase forming a rock-salt-type (OR)(RO) structure whereas the T′ phase contains anions at the positions tetrahedrally coordinated by four R^{3+} cations (fluorite type (R)(O_2)(R) structure). Therefore, both phases mainly differ by the anion distribution in the R_2O_2 blocks; occupied anion positions in the T phase are vacant in the T′ phase and vice versa (Fig. 1).

Upon variation of cation and anion composition, the stability ranges of the T and T′ structures are determined by the match between the R_2O_2 blocks and the perovskite (CuO_2) layers. The in-plane dimensions of the R_2O_2 block depend on the type and the ionic radius of the rare earth cation, while the planar Cu–O distance can be altered by the degree of filling of the antibonding σ^* band formed by the $3d_{x^2-y^2}$ orbitals of copper and the $2p_{x,y}$ orbitals of oxygen. The Cu–O bonds may expand or contract by adding or removing electrons from the σ^* band (decreasing or increasing the formal copper valence) (1).

The transformation of a rock salt slab to a fluorite-type structure is accompanied by a significant expansion in the *ab*-plane as was found for solid solutions of $La_{2-x}Nd_xCuO_4$. The subcell a parameter increases from $a = 3.801$ Å to $a = 3.991$ Å upon transformation from T to T′ for $x > 0.5$ (2). Thus the reduction of the Cu atoms (and an increase of the Cu–O distance) may result in the transformation of the T structure to the T′ type whereas the oxidation is favorable for the formation of the T phase. This is the case for the $La_{1.5}Nd_{0.5}CuO_{4+\delta}$ compound which adopts a T type structure for $\delta = +0.01$ and a T′ structure for $\delta = -0.02$ (3). Indeed, the T phases convert to a superconducting state when holes are created in the σ^* band (p-doping) but in the T′ materials a reduction of Cu (n-doping) induces superconductivity. Such a reductive treatment was performed by the heterovalent replacement of one O^{2-} by one F^- (4–6) or by a combination of substitutions in the cation and the anion sublattices (7). An XAFS study (8) showed that the majority of the fluorine substitutes oxygen at the fluorite-type site in the Nd_2O_2 slab, which does not significantly influence the crystal

[1]To whom correspondence should be addressed. Fax: +32/32180318. E-mail: johader@ruca.ua.ac.be.

0022-4596/01 $35.00

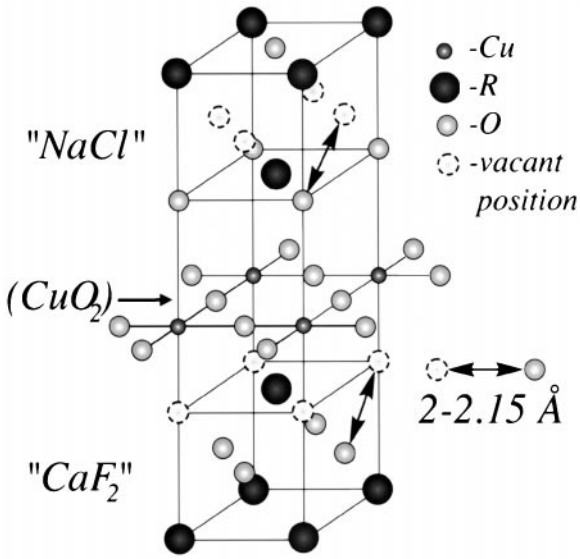

FIG. 1. Scheme of intergrowth between perovskite-type (CuO_2) layers, rock salt ("NaCl"), and fluorite-type ("CaF_2") R_2O_2 blocks.

structure and does not cause the appearance of lattice distortions or structural modulations (9, 10).

In contrast to an anion replacement, an insertion of additional anions into the R_2CuO_4 structures is accompanied by a structural transformation. If both the positions in the octahedral and the tetrahedral interstices of the R_2O_2 slab are simultaneously occupied, the structure of the initial oxide undergoes significant deformations to diminish the repulsion forces between neighboring anions separated by distances as short as 2–2.15 Å (Fig. 1). Recently we showed that the soft fluorine insertion into La_2CuO_4 and $LaHo_{0.75}Sr_{0.25}CuO_{3.9}$ (T* type structure) results in anion rearrangements between the two possible positions in the R_2O_2 blocks, creating numerous structures which can be considered as intermediate ones between T and T′ types (11, 12). The highly fluorinated $La_2CuO_{3.6}F_{0.8}$ phase exhibits an ordered alternation of fluorite-type and rock-salt-type slabs, not only along the *c*-axis but also within the *ab*-plane. As a result the octahedral coordination of some of the Cu ions is transformed into a square pyramidal one (11). The formation of a monoclinic superstructure in the fluorinated $LaHo_{0.75}Sr_{0.25}CuO_{3.9}$ is accompanied by an equal anion arrangement within the initially different fluorite and rock salt blocks (12). We can also expect that the presence of additional interstitial anions may lead to significant structural changes in the fluorinated T′ phase. A filling of the rock salt positions due to a partial migration of anions from the fluorite sites and an intercalation of fluorine is favorable for an increase of the formal copper valence and may create the conditions necessary for *p*-type superconductivity.

In this contribution we report on the structure of fluorinated Nd_2CuO_4 prepared by a soft chemistry technique using XeF_2 as a fluorinating agent.

2. EXPERIMENTAL

Nd_2CuO_4 for further fluorination was prepared by a routine ceramic technique using Nd_2O_3 and CuO as initial materials. A stoichiometric mixture of these oxides was ground, pelletized, and fired at 950°C for 2 days. The prepared single-phase material has cell parameters as listed in Table 1.

The operations with XeF_2 were carried out in a glove box filled with dried N_2. Nd_2CuO_4 (0.4 g) was mixed with XeF_2 (provided by the Laboratory of Inorganic Synthesis of the Institute of Applied Chemical Physics, "Kurchatovskii Institut", Moscow, Russia) in molar ratios of 1:0.5 and 1:1 and ground in an agate mortar. The mixture was placed in a Ni crucible and then sealed in a N_2-filled copper tube. The samples were annealed at 300°C, 400°C, and 500°C for 20 h and then furnace-cooled to room temperature.

The phase composition of the samples and the lattice parameters of the compounds were determined by X-ray diffraction using a focusing Guinier camera FR-552 ($CuK\alpha_1$ radiation, germanium internal standard) and a STADI P difractometer ($CuK\alpha_1$ radiation, transmission geometry, linear PSD).

The temperature dependence of the AC susceptibility was measured in the range of 12–100 K at an external field amplitude of 1 Oe and a frequency of 27 Hz. The formal copper valence was determined by iodometric titration.

Electron diffraction (ED) and high-resolution electron microscopy (HREM) were performed with a JEOL 4000EX microscope. EDX analysis and electron diffraction were performed using a Philips CM20 microscope with a LINK-2000 attachment. Simulations of the HREM images were performed using the MacTempas software.

RESULTS

The cell parameters of Nd_2CuO_4 fluorinated at different temperatures and with different amounts of XeF_2 are listed

TABLE 1
Fluorination Conditions, Cell Parameters, and Formal Copper Valence for Initial and Fluorinated Samples

No.	Fluorination conditions	*a*, Å	*c*, Å	V_{Cu}
1	Initial	3.9423(2)	12.1667(7)	+2.00
2	300°C, 10 h, 0.5 XeF_2	3.9378(5)	12.1545(7)	+2.01
3	300°C, 20 h, 1 XeF_2	3.9366(3)	12.1539(12)	+2.03
4	400°C, 20 h, 1 XeF_2	3.9409(2)	12.1590(5)	+1.95
5	500°C, 20 h, 0.5 XeF_2	3.9488(5)	12.126(2)	

in Table 1. Samples 2–4 exhibit the T′ structure and only insignificant impurity peaks with a relative intensity less than 5% were found. The X-ray diffraction pattern of sample 5 shows the presence of broad and intense reflections of NdOF, indicating the partial decomposition of Nd_2CuO_4 under fluorination. Superconductivity was not detected in any of the fluorinated samples.

Samples 3 and 4 were investigated by electron microscopy to determine the influence of fluorination on the structure of the T′ phase. Several clearly different sets of diffraction patterns (DPs) were observed. The first set of patterns closely resembles those of the initial material and could be indexed with the cell parameters determined from X-ray diffraction (Table 1). The second set of DPs shows the presence of superstructure reflections in the [110]* zone at the $(h + 1/2, k + 1/2, l)$, $l = 2n + 1$ positions (Fig. 2a). The $[\bar{1}10]$* zone of this set shows no additional reflections, but a deviation from 90° can be seen between the vectors [001]* and [110]* (Fig. 2b) indicating a monoclinic distortion. We will further refer to this monoclinic structure using subscript M, and to the initial tetragonal structure with subscript T. To index these diffraction patterns, a new monoclinic unit cell should be used, with $[\bar{1}10]$* as the direction of basic vector b^*_M. The relations between the vectors of the tetragonal unit cell and the new monoclinic one are given by $[100]^*_M = [001]^*_T$, $[010]^*_M = [\bar{1}10]^*_T$, and $[001]^*_M = [110]^*_T$, ($a_M \approx 12.96$ Å, $b_M \approx 5.5$ Å, $c_M \approx 5.8$ Å, and $\beta \approx 92°$). After reindexing the patterns of Fig. 2 in the monoclinic system, it was found that the reflections on these DPs obey the extinction conditions compatible with the space groups *Cc* or *C*2/*c*: hkl, $h + k = 2n$; $h0l$, $l = 2n$. Splitting of the basic spots along the a^*_M axis is visible on Fig. 2a; the superlattice spots however remain unsplit. This splitting arises due to the considerably different repeat periods for the initial phase ($c = 12.1667(7)$ Å) and the fluorinated phase ($a_M \approx 12.96$ Å) along this direction. Hence this diffraction pattern can be interpreted as the superposition of $[001]^*_M$ and $[110]^*_T$ DPs. The $[001]_M$ low-magnification multibeam image (Fig. 3) confirms the coexistence of both phases in one crystallite and shows the formation of narrow bands of the monoclinic phase in a matrix of initial T′ phase. The simultaneous presence of both the monoclinic and tetragonal phases in the region shown in Fig. 3 was proven by ED and HREM observations performed before taking the low-magnification image.

The presence of fluorine in the samples was verified using EDX analysis. Figure 4 represents the typical EDX spectrum frequently observed on different crystallites showing regions such as seen on Fig. 3 and clearly demonstrates the presence of fluorine peaks. Unfortunately, the intimate intergrowth of the monoclinic and tetragonal domains hampers the separate EDX analysis of these phases. An exact quantitative measurement of the fluorine content is difficult because of the low *Z*-number.

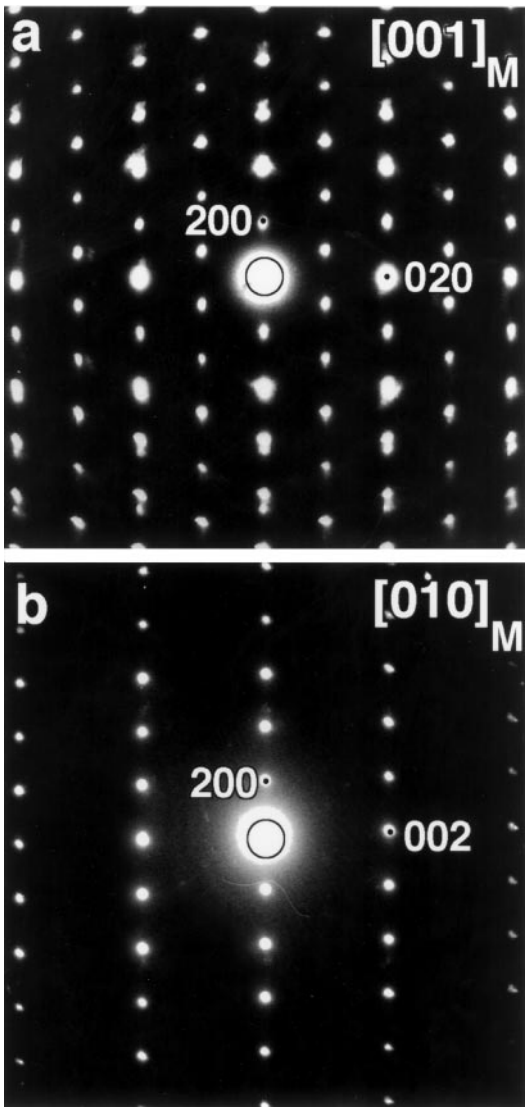

FIG. 2. Electron diffraction pattern of the $[001]^*_M$ (= $[110]^*_T$) and $[010]^*_M$ (= $[\bar{1}10]^*_T$) zones taken from areas of the monoclinic phase. The relations between the reflections in monoclinic and tetragonal lattices are $200_M = 002_T$, $020_M = \bar{1}10_T$, and $002_M = 110_T$.

Figure 5 shows a HREM image of the monoclinic phase with a boundary between domains in $[001]_M$ and $[010]_M$ orientations. The interface plane is roughly parallel to $[100]_M$. This domain boundary is clearly introduced by the lowering of the symmetry. In the tetragonal phase both domains would be equivalent and $[110]_T$ oriented. The image contrast in the $[010]_M$ domain is similar to that for nonfluorinated Nd_2CuO_4, except for the oblique angle between the $[100]_M$ and $[001]_M$ directions. In the $[001]_M$ domain the superstructure can be detected by the alternation of dark and bright spots along the $[010]_M$ direction. On the computer-simulated Fourier transformations, shown in the inset of Fig. 5, the superstructure in $[001]_M$ and the

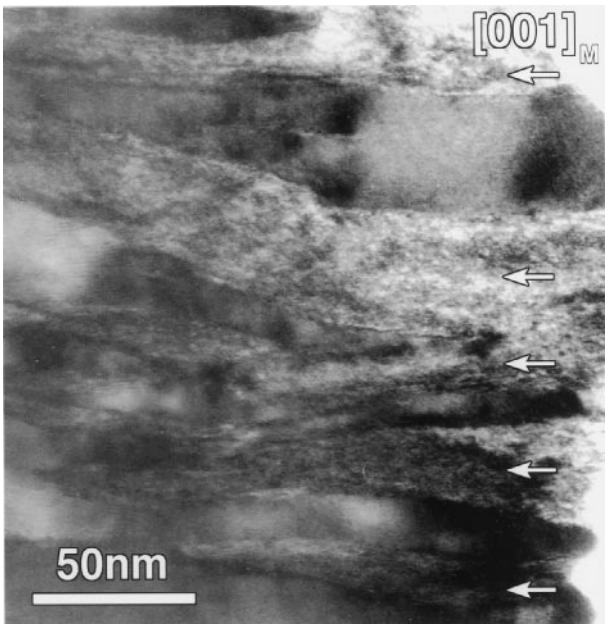

FIG. 3. Low-magnification multibeam $[001]_M$ image showing the coexistence of the tetragonal and monoclinic phases. The monoclinic domains are marked by arrows.

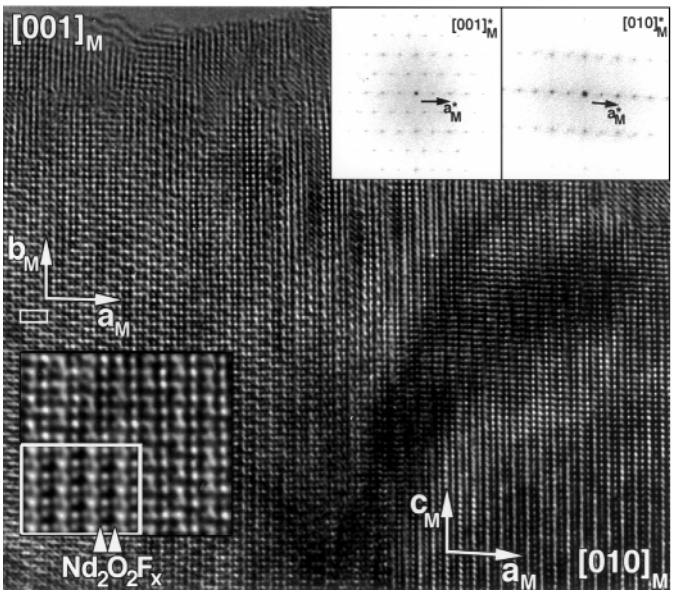

FIG. 5. High-resolution electron microscopy image of the monoclinic phase, taken along the $[001]_M$ (at the left side) and $[010]_M$ (at the right side) directions. Fourier transforms of both areas are shown. An enlarged area of the experimental $[001]_M$ image is inserted with the simulated pattern ($\Delta f = +15$ nm and $t = 9$ nm) in the white frame.

oblique angle between $[001]_M$ and $[100]_M$ are clearly visible. The superstructure is unstable under the intense electron beam used for HREM imaging and fades away after approximately 10 s.

DISCUSSION

Our previous investigations of different complex copper oxyfluorides revealed several features of the interaction of XeF_2 with the initial material. The behavior of Nd_2CuO_4 under fluorination confirms the conclusions made after investigation of other fluorinated cuprates (11, 12). The increase of the formal copper valence under fluorination takes place due to the intercalation of fluorine into the structure of the initial oxide. The changes in the cell parameters of the fluorinated Nd_2CuO_4 phase correlate well with the formal copper oxidation state V_{Cu} determined by iodometric titration. In the first stage (300°C, samples 2 and 3) an anion insertion takes place, resulting in an increase of V_{Cu}, accompanied by a contraction of the *a* parameter. The interaction of Nd_2CuO_4 with XeF_2 at 300°C results in oxidation of the Cu atoms due to the following reaction:

$$Nd_2CuO_4 + 0.5xXeF_2 \rightarrow Nd_2CuO_4F_x + 0.5xXe.$$

It is reasonable to suggest a competing reaction taking place together with the fluorine insertion during the fluorination in the closed Cu vessel at 400–500°C (samples 4 and 5). At increased temperatures an anion exchange with replacement of oxygen by fluorine dominates, leading to a reduction of the Cu cations, an expansion of the unit cell in the *ab*-plane, and a release of oxygen:

$$Nd_2CuO_4 + xXeF_2 \rightarrow Nd_2CuO_{4-x}F_{2x} + xXe + x[O].$$

The oxygen released during this process is adsorbed at the inner walls of the Cu tube, forming Cu_2O. The rare-earth elements form fluorides and oxyfluorides with extremely high lattice energies and which are, consequently,

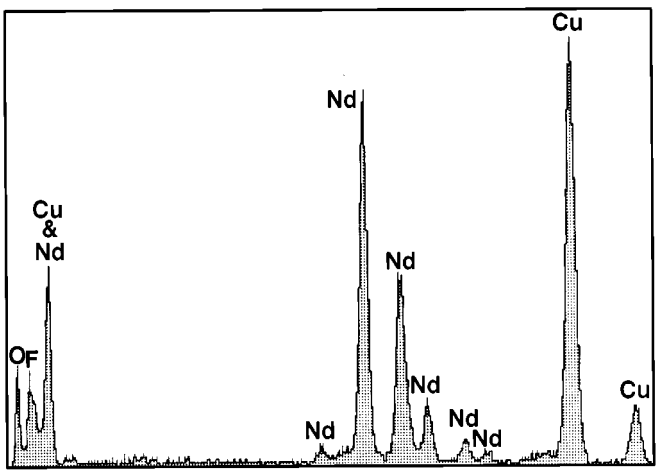

FIG. 4. EDX spectrum of the fluorinated T′ phase.

thermodynamically very stable. Therefore the equilibrium stage of the fluorination reaction is a decomposition of the initial oxides. The partial decomposition of Nd_2CuO_4 with the formation of NdOF was indeed observed at 500°C and it can be considered as the final stage of the fluorination reaction.

The fluorine insertion at low temperature occurs very inhomogeneously, resulting in the formation of domains with a different level of fluorination. In most cases the phase with the lower fluorine content shows only minor deviations from the structure of the initial cuprate, whereas the highly fluorinated material exhibits significant structure transformations. The fluorination of related structures such as the T phase La_2CuO_4 (11) and the T* phase $LaHo_{0.75}Sr_{0.25}CuO_{3.9}$ (12) showed that mostly the R_2O_2 slabs are affected by fluorination and that the (CuO_2) layers undergo only slight deformations. It is therefore reasonable to expect that the vacant anion positions in the Nd_2O_2 slab of the T′ phase would accommodate extra anions.

TEM investigations of the samples fluorinated at 300°C and 400°C reveal a new fluorinated superstructure, having a monoclinic unit cell with $a_M \approx c$, $b_M \approx a\sqrt{2}$, $c_M \approx a\sqrt{2}$. This phase forms as narrow bands within the matrix of the undistorted T′ structure and, probably, the small width of these bands is responsible for the absence of the reflections corresponding to the monoclinic phase on the X-ray powder diffraction patterns. To determine the origin of the superstructure, experimental images based on different models were compared with computer-simulated images. Using the most symmetrical space group determined from electron diffraction, $C2/c$, different possible models of anion ordering can be built. Due to the small scattering power of O^{2-} and F^- and the negligible difference between them, it was not possible to determine the exact distribution of oxygen and fluorine between different anion sites nor the occupancy factors of these positions. The proposed structure of Fig. 6 can therefore only be considered as a rough model for the crystal structure of the monoclinic phase. The best agreement between experimental and calculated images was obtained when an ordered, partial occupation of the anion positions tetrahedrally coordinated by Nd cations was assumed (Fig. 6a). Anions at these positions form chains along the c_M-axis and alternate with chains of vacant sites. Since we assumed an excess of anions in comparison with the ideal stoichiometry, the remaining fluorine and oxygen atoms were located at the positions completing the copper coordination environment from square to octahedron (rock salt positions). An octahedral coordination of Cu cations should result in an elongation of the apical Cu–O distances due to the Jahn–Teller effect, which explains the considerable increase in the c parameter which was experimentally observed for this phase. The simultaneous occupation of the rock-salt- and the fluorite-type positions leads to short anion–anion distances that can be overcome by a tilt of the

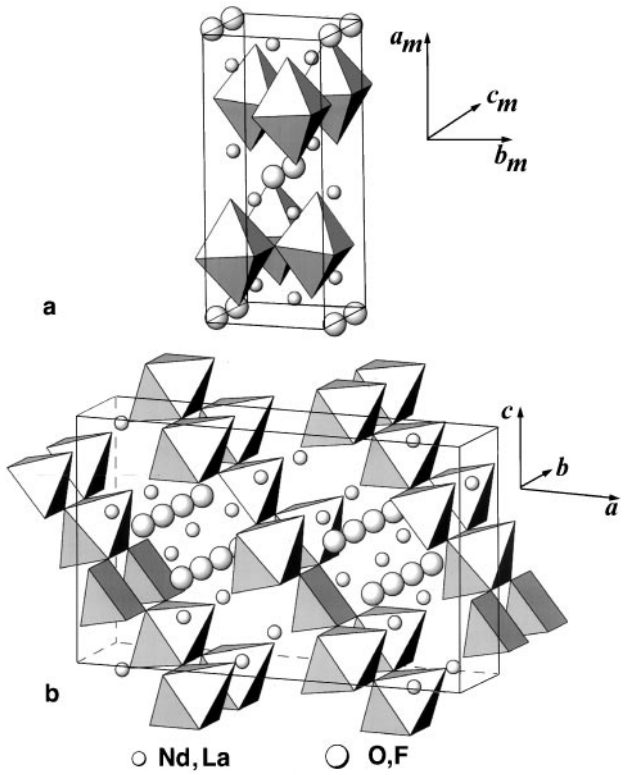

FIG. 6. Structure model for the $Nd_2Cu(O, F)_{5-\delta}$ phase (a). Cu atoms are located at the centers of the octahedra. The crystal structure of $La_2CuO_{3.6}F_{0.8}$ (b). Note the alternation of vacant and filled fluorite-type positions along [110] of the K_2NiF_4 subcell.

(CuO_6) octahedra around $[001]_M$ in order to decrease the repulsion between the anions. The nominal composition of the monoclinic phase, as deduced from the model, would be $Nd_2Cu(O, F)_{5-\delta}$. According to the results of the iodometric titration, the formal valence of the Cu atoms is close to $V_{Cu} = +2$, which leads us to propose the $Nd_2CuO_3F_2$ composition, assuming a full occupancy of the anion positions in the structure model considered above. However, the exact fluorine and oxygen content is uncertain, as it cannot be deduced from EDX, nor from HREM image simulations.

The simulated image, inserted in the high-resolution image of Fig. 5, was obtained for a defocus value $\Delta f = +15$ nm and a thickness $t = 9$ nm, and was found to be in good agreement with the experimental image.

The structure of the monoclinic fluorinated Nd_2CuO_4 shows close resemblance with the $La_2CuO_{3.6}F_{0.8}$ structure (Figs. 6a and 6b); both can be considered as intermediate between the structures of the T and T′ types and can be compared with the T* structure. The structure of the T* compounds is the result of an intergrowth of fragments of T and T′ material where R_2O_2 layers of a fluorite and a rock salt type alternate along the direction normal to the (CuO_2) planes. In contrast to this, for the $La_2CuO_{3.6}F_{0.8}$ and

$Nd_2Cu(O,F)_{5-\delta}$ structures the fluorite and rock salt fragments alternate not only along the [001] direction of the K_2NiF_4-type subcell, but also in the *ab*-plane along the [110] direction. The increase of the repeat period along the stacking axis from 12.17 Å for the initial Nd_2CuO_4 to 12.96 Å for the fluorinated monoclinic $Nd_2Cu(O,F)_{5-\delta}$ is in agreement with the appearance of rock-salt-type blocks in the structure. The ratio of the cell dimensions for the K_2NiF_4-type subcell of $Nd_2Cu(O,F)_{5-\delta}$, $c/3a = 1.08$, corresponds to the range of $c/3a$ ratios found for the T* phases ($c/3a \approx 1.15$ for the T phases, $c/3a \approx 1.06$–1.08 for the T* phases, and $c/3a \approx 1.02$ for the T′ phases (1)), thus outlining the similarity between these structures.

The maximal formal copper valence $V_{Cu} = +2.03$ achieved by the fluorination is not sufficient for the appearance of superconducting properties. For instance, superconductivity was found in the T* phase $La_{0.9}Sm_{0.9}Sr_{0.2}CuO_{4+\delta}$ only after a copper valence of $+2.13$ was reached by high-pressure oxygen treatment, whereas no superconducting transition was observed at $V_{Cu} = +2.07$ (13). In the case of fluorinated Nd_2CuO_4 the highest copper oxidation state is even lower which should suppress the superconductivity.

ACKNOWLEDGMENTS

This work was performed in the framework of IUAP-PAI 4/10 of the Belgian government and partially supported by INTAS-99-1136 and Volkswagen grant I/75849.

REFERENCES

1. A. M. Abakumov, E. V. Antipov, L. M. Kovba, E. M. Kopnin, S. N. Putilin, and R. V. Shpanchenko, *Russ. Chem. Rev.* **64,** 719–729 (1995).
2. F. Arrouy, A. Wattiaux, C. Cros, G. Demazeau, J.-C. Grenier, M. Pouchard, and J. Etourneau, *Physica C* **175,** 342–346 (1991).
3. J. F. Bringley, S. S. Trail, and B. A. Scott, *J. Solid State Chem.* **88,** 590–593 (1990).
4. A. C. W. P. James, S. M. Zahurak, and D. W. Murphy, *Nature* **338,** 240–241 (1989).
5. U. Asaf, O. Cohen, I. Felner, and U. Yaron, *Physica C* **209,** 183–186 (1993).
6. A. Tighezza, J. L. Rehspringer, and M. Drillon, *Physica C* **198,** 209–214 (1992).
7. U. Asaf, I. Felner, and U. Yaron, *Physica C* **211,** 45–48 (1993).
8. A. Krol, Y. L. Soo, Z. H. Ming, S. Huang, Y. H. Kao, G. C. Smith, K. Lee, A. C. W. P. James, and D. W. Murphy, *Phys. Rev. B* **46,** 443–447 (1992).
9. J. Sugiyama, M. Kosuge, Y. Ojima, H. Yamauchi, and S. Tanaka, *Physica C* **179,** 131–137 (1991).
10. C. H. Chen, D. J. Werder, A. C. W. P. James, D. W. Murphy, S. Zahurak, R. M. Fleming, B. Batlogg, and L. F. Schneemeyer, *Physica C* **160,** 375–380 (1989).
11. A. M. Abakumov, J. Hadermann, G. Van Tendeloo, R. V. Shpanchenko, P. N. Oleinikov, and E. V. Antipov, *J. Solid State Chem.* **142,** 440–450 (1999).
12. J. Hadermann, A. M. Abakumov, O. I. Lebedev, G. Van Tendeloo, M. G. Rozova, R. V. Shpanchenko, B. Ph. Pavlyuk, E. M. Kopnin, and E. V. Antipov, *J. Solid State Chem.* **147,** 647–656 (1999).
13. E. M. Kopnin, E. V. Antipov, L. M. Kovba, P. E. Kazin, V. A. Rybachuk, V. V. Moshalkov, and A. E. Kachanovsky, *Superconductivity*: *Phys. Chem. Technol.* (*Russ.*) **5,** 530–539 (1992).